Monte Carlo Simulations of Size and Structure of Gel Precursors in Silica Polycondensation

Ján Šefčík*,† and Stephen E. Rankin*,‡

Swiss Federal Institute of Technology Zürich, Laboratorium für Technische Chemie, ETH Hönggerberg/HCI, CH-8093 Zürich, Switzerland, and Chemical and Materials Engineering Department, University of Kentucky, 177 Anderson Hall, Lexington, Kentucky 40506-0046

Received: June 21, 2002; In Final Form: October 21, 2002

Sol−gel processing provides a useful route to novel metastable materials such as molecular hybrids of silica and either transition metal oxides or organic components. Because the properties of these materials depend critically on how the components are combined, we present calculations of the size and structure of silica building blocks that may be prepared as precursors to nanocomposites. By fitting existing silicon-29 NMR data, we find kinetic parameters applicable for acid catalyzed hydrolytic polycondensation of tetraethoxysilane and tetramethoxysilane precursors. In a wide range of conditions, the local connectivity of silicon sites evolves in approximately the same way with respect to the siloxane bond conversion. Using dynamic Monte Carlo simulations, including nearest-neighbor effects and cyclization, we calculate the molecular weight distribution of silica as a function of conversion, in reasonable agreement with available experiments. At low siloxane bond conversions ($\alpha \leq 0.6$) the mass weighted degree of polymerization DP_w is less than 10. When enough water for alkoxide hydrolysis is available, gel precursors containing 8−20 silicon sites form quickly up to conversion $\alpha = 0.65-0.75$ and then slowly react together until gelling at $\alpha = 0.82$. The calculated distributions provide a quantitative road map for forming composite materials with well-defined silica blocks, where the siloxane bond conversion can be used as an indicator of the progress of structure development.

Introduction

Sol−gel silica, prepared by hydrolytic polycondensation of high-purity alkoxysilane precursors, is of high interest as a source of novel materials. This interest falls into three categories: controlled mesoporous silica formed through surfactant "templating", highly dispersed organic−inorganic hybrid materials, and metastable mixed oxides.

The first class of materials has seen much technological innovation since the original work of Kresge et al.[1] Prior to the discovery of ordered mesoporous silica, porous silicas were either dried gels[2] of well-defined but relatively broad pore size distribution (microporous or mesoporous), or crystalline microporous molecular sieves.[3] The addition of structure-directing agents such as surfactants to these solutions has led to the formation of mesoporous silicas with a variety of ordered pore structures,[4,5] but with many untested hypotheses about their route of formation. One important unanswered question is exactly what silica species are present during the formation of these materials at low pH. Without this information, the influence of the silicates on the formation of lyotropic liquid crystals, or on the nucleation of an ordered structure, cannot be addressed fully. Nor can the competition between polymerization of the silica and formation of a lyotropic liquid or solid crystalline phase.

Similar questions arise in the formation of organic−inorganic hybrid materials containing silica. By adding organically modified alkoxysilanes or simply organic polymers to tetraethoxysilane during sol−gel processing, a wide range of hybrid materials has been synthesized.[6] The state of the silica during this process is important for two reasons: First, the silica may not be miscible with the organic component and therefore may undergo phase separation at some point during the processing.[7] The point at which this occurs should be strongly influenced by the structure distribution of the silica. Second, the size of the silica domains in the hybrid will have a large impact on the performance of the material. Therefore, it is important to know the structure of the silica species present before and after addition of the organic component.

In the final class of materials, mixed oxides, the distribution of metal ions strongly influences the activity, properties, and stability of the material. Some of these mixed oxides are of interest for their acidic properties—properties that arise from charge imbalances across M−O−M′ bonds.[8] To prepare a catalyst with the maximum density of these acid sites, one must control the co-gelation process through which they are prepared.[9] Homogeneity in the distribution of silica with other metal oxides plays an important role in the texture and crystal structure development of catalysts and ceramics. All of these features are related to the polymerization behavior of silica in the precursor sol.

Although silica polymerization plays a central role in all of these materials, the state of the silica during the synthesis is frequently unknown. In this contribution, we will model polycondensation of the silica precursors alone, prior to the addition of other components. As we will discuss, it is not unusual in nanocomposite synthesis procedures to find a step where silica polymerizes alone for a certain time. We will present new calculated molecular weight distributions of silicate oligomers formed during acid-catalyzed alkoxysilane polymerization. We propose that these distributions can be used as an aid to developing new materials when silica reacts for some time on its own, but limited information about reaction extent

* To whom correspondence should be addressed.
† ETH Zürich. E-mail: sefcik@tech.chem.ethz.ch.
‡ University of Kentucky. E-mail: srankin@engr.uky.edu.

10.1021/jp026361d CCC: $25.00
Published on Web 12/10/2002

(such as the siloxane bond conversion or the fraction of monomer consumed) is available.

Though this paper will focus on calculated results, we will relate the calculations to a body of existing experiments. We will determine the kinetic parameters needed for our models from a composite set of ^{29}Si NMR data on silicon connectivity and gelation conversion and discuss the validity of simplified models. Then we will apply our models to calculate molecular weight distributions and the weight average degree of polymerization as a function of siloxane bond conversion and compare our results to available experimental data.

Background

Hydrolysis. Strategies to promote homogeneity in molecular composites containing silica often focus on differences in hydrolysis rate. In mixed metal oxides, this focus is appropriate given the large discrepancies of hydrolysis reactivity of transition metal alkoxides and silicon alkoxides.[10] A popular strategy is to "prehydrolyze" the silicon alkoxide prior to the addition of a transition metal.[11] Usually, this "prehydrolysis" is performed for several minutes in an acidic environment. If this step is very short, only hydrolysis reactions will occur, and the competition between sequential hydrolysis steps will determine the distribution of partially hydrolyzed monomers available for further reactions. The kinetics of hydrolysis and re-esterification of silicon alkoxides have been thoroughly characterized.[12]

However, if enough time is allowed so that condensation begins, it is rate limiting at low pH (pH < 4)[2]. In this case, hydrolysis (eq 1) will be fast enough (and reversible enough) to reach pseudoequilibrium. Beyond this point, the fraction of hydrolyzed ethoxysilane groups available for reaction is a function only of the total amount of water added and the siloxane bond conversion.

$$\equiv\text{SiOR} + \text{H}_2\text{O} \overset{K_h}{\longleftrightarrow} \equiv\text{SiOH} + \text{ROH} \quad (1)$$

$$\equiv\text{SiOH} + \text{HOSi}\equiv \rightarrow \equiv\text{SiOSi}\equiv + \text{H}_2\text{O} \quad (2)$$

Hydrolysis equilibrium coefficients of ethoxysilanes (eq 1) have been found to vary only in a small range about a value of $K_h = 18$, regardless of hydrolysis degree, connectivity, or organic substitution.[13] Here, we will assume that this is true, in which case the equilibrium of eq 1 yields an easily solved quadratic equation (eq 3) for the dependence of the average hydrolysis extent, χ, on condensation (eq 2) conversion, α.

$$K_h = \frac{[\text{SiOH}][\text{ROH}]}{[\text{SiOR}][\text{H}_2\text{O}]} = \frac{\chi([\text{ROH}]_0/[\text{SiOR}]_0 + \chi(1-\alpha) + \alpha)}{(1-\chi)([\text{H}_2\text{O}]_0/[\text{SiOR}]_0 - \chi(1-\alpha) - \alpha/2)} \quad (3)$$

where $\chi = [\text{SiOH}]/([\text{SiOH}] + [\text{SiOR}])$, $\alpha = [\text{SiOSi}]/(f[\text{SiOR}]_0/2)$, and f is the functionality of the monomer, in this case 4.

Connectivity Distributions in Homogeneous Systems. When "prehydrolysis" is carried out for a long time, or at high acidity, it is likely that alkoxysilanes not only undergo hydrolysis but also grow during their processing. When condensation is rate-limiting, hydrolysis steps play little role in the development of siloxane structure.[14] Instead, the sequence of condensation steps determines the distribution of siloxane structures available for reaction and co-assembly with other metal oxides, organic units, or structure-directing agents. Therefore, we will discuss in detail the condensation reactivity of alkoxysilane precursors.

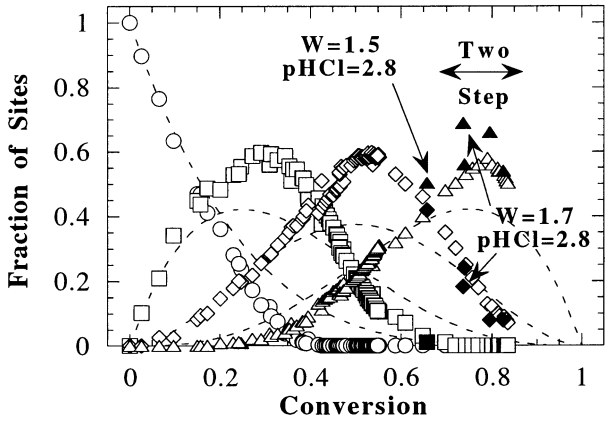

Figure 1. Connectivity (Q_i) distribution as a function of siloxane bond conversion for homogeneous tetraethoxysilane systems. Open symbols are combined data from Devreux et al.[15] and Sanchez et al.[29] They represent Q_0 (○), Q_1(□), Q_2 (◇), and Q_3 (△) sites. Filled symbols are data from Brinker and Assink[17] and Brinker et al.[16] for systems under the indicated conditions. They represent Q_1 (■), Q_2 (◆), and Q_3 (▲) sites. See Table 1 for more details on conditions.

TABLE 1: Solution Composition for Sol−Gel Recipes with Tetraethoxysilane

reference	[TEOS] (M)	$W = H_2O/TEOS$	pHCl
Brinker et al.[16]	1.9	5.1	1.0
Brinker and Assink[17]	2.3	1.5	2.8
Brinker and Assink[17]	2.3	1.7	2.8
Devreux et al.[15]	1.3	10	3[a]
Kopylov et al.[47]	2.3	0.2−1.5	2.3
Sanchez et al.[29]	2.1	2.0	2.6

[a] Estimated equivalent.

A number of researchers have measured, using ^{29}Si nuclear magnetic resonance (NMR), the evolution of the connectivity distribution of silicates as a function of time, or as a function of the siloxane bond conversion α. This distribution is defined by the fractions of silicon sites with different numbers (i) of siloxane bonds to other silicon sites, Q_i.

The most frequently investigated cases of alkoxide hydrolytic polycondensation are acid-catalyzed. In these conditions, polymerization is slow and the systems remain homogeneous through gelation. Figure 1 summarizes the evolution of the Q_i distribution for polymerizing tetraethoxysilane (TEOS) measured by ^{29}Si NMR by several investigators.[15−17,29] The conditions under which these data were collected are summarized in Table 1. In none of these cases does the total integrated intensity of the ^{29}Si NMR spectra decrease, indicating that precipitation does not occur.

Despite the range of conditions represented (1 < pH < 3 and 1.5 < W < 10), all of the data plotted in Figure 1 fall in a relatively narrow range. Surprisingly, a similar trend in connectivity distribution is also observed for polymerizing tetramethoxysilane[18−22] (TMOS), as shown in Figure 2. Table 2 summarizes the conditions for the TMOS experiments. These data cover a range of pH from 1.7 to 2.8. Given the similarity of the connectivity distributions of tetraethoxysilane and tetramethoxysilane polycondensation under a wide range of conditions, the distribution seems universal for homogeneous gels. This implies two things about the structure of homogeneous silica sols.

First, it should be possible, using a less elaborate and faster technique than ^{29}Si NMR, to identify siloxane bond conversion α to obtain a good estimate of the connectivity distribution of a homogeneous silica sol. In the absence of a direct measurement

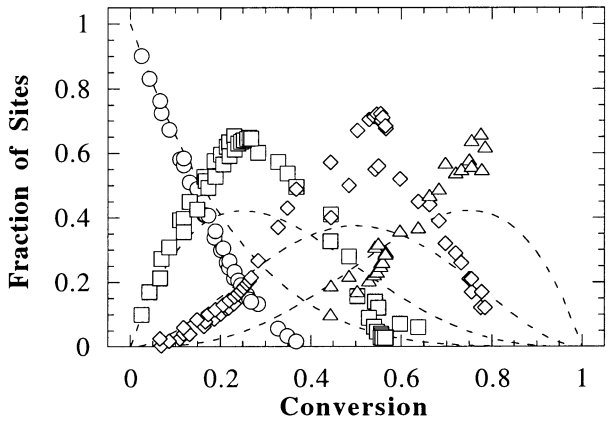

Figure 2. Connectivity (Q_i) distribution as a function of siloxane bond conversion for homogeneous tetramethoxysilane systems. The data (symbols) are compiled from several sources[18−22] where the pHCl is between 1.7 and 2.8. The meaning of the symbols is the same as in Figure 1. See Table 2 for more details on conditions.

TABLE 2: Solution Composition for Sol−Gel Recipes with Tetramethoxysilane

reference	[TMOS] (M)	$W = H_2O/TMOS$	pHCl
Assink and Kay [22]	2.2	1.0	2.8
Brunet et al.[19]	2.3	8.0	2.0
Brunet and Cabane [21]	3.2	1.0	2.8
Kelts et al.[18] (with D_2O)	2.9	2.6	1.7
Kelts et al.[18] (with D_2O)	2.9	2.6	2.7
VanBeek et al.[20]	2.2	8.0	2.7

of the siloxane bond concentration, α can be found from two linearly independent concentrations or concentration ratios. For instance if the ratio of alcohol to silicon (A) and of water to silicon (W) can be determined by FTIR, ^{1}H NMR, or a fluorescent probe molecule,[23] then solving stoichiometric relations for the water and alcohol concentrations give

$$\alpha = (A - A_0 + W - W_0)/2 \tag{4}$$

where a subscript zero indicates the initial value.

Second, the universality of the connectivity distribution in these systems implies that the structure evolution should be similar. The simulated results for molecular structure distribution, discussed below, should therefore be applicable to other homogeneous silica sols. A good model of tetraalkoxysilane polymerization should be able to provide a road map for the structure distribution of silicates where only α is needed as a navigational aid.

Flory−Stockmayer Random Branching. Classical random branching theory (concurrently developed for nonlinear polycondensation by Flory[24] and Stockmayer[25]) provides closed expressions for the average properties of the system. It has been shown to be consistent with the molecular weight distribution,[26] average degrees of polymerization,[27] and fractal dimension[28] of acid-catalyzed silica gels as long as one assumes that the functionality of the monomer is just above 2.

This is not consistent with the actual functionality of the monomer (4). It had been proposed that limited hydrolysis may be responsible for reducing the effective functionality of the monomer, but detailed kinetic and thermodynamic investigations have disproved this hypothesis. There are no special kinetic or thermodynamic limitations on the actual functionality of the monomer.[12]

Other kinetic investigations have also demonstrated that the condensation reactivity assumptions inherent in the Flory−Stockmayer theory do not hold for this system. This can be qualitatively seen by comparing the data (points) in Figure 1 to the predictions from random branching theory (dashed lines). The curve for each intermediate site is more sharply peaked than random branching predicts. This indicates that those species accumulate before being consumed by the next reaction in the sequence; in other words, condensation appears to become slower for each site as siloxane bonds are added. This trend has been verified by fitting polycondensation models with first-shell substitution effects[19,29,30] and cyclization[31,32] (see below) to ^{29}Si NMR data. The same trend appears to be true for tetramethoxysilane-derived silicates, as shown in Figure 2.

Still, the closed form solutions of the theory are useful for rapid calculation, so we will discuss under what conditions Flory−Stockmayer random branching provides an adequate approximate model of sol−gel silica polymerization. The expressions that we will use (derived elsewhere[33,34]) are the dependence of the weight-average degree of polymerization, DP_w, on condensation conversion, α (eq 5) and the dependence of the weight fraction of each species, W_i for species i, on the condensation conversion (eq 6).

$$DP_w = \frac{1+\alpha}{1-(f-1)\alpha} \tag{5}$$

$$W_i = i\frac{[(f-1)i]!}{[(f-2)i+2]!i!}\frac{(1-\alpha)^2}{\alpha}[\alpha(1-\alpha)^{f-2}]^i f \tag{6}$$

First-Shell Substitution Effects (FSSE). Pouxviel and Boilot,[35] and Kay and Assink[36] first proposed that the reactivity of silicon sites should depend at least on the identity of the nearest neighbors attached to each site. This means that each hydrolysis and each condensation step should have a different rate coefficient depending on the identities of the four neighbors of each silicon. With the hydrolysis pseudoequilibrium assumption, it is possible to focus only on the condensation reactivity trends by rewriting condensation reactions in the form of eq 7 and the bimolecular condensation rate expressed by eq 8.

$$Q_i + Q_j \xrightarrow{k_{ij}} Q_{i+1} + Q_{j+1} + H_2O \tag{7}$$

$$R_{ij} = k_{ij}\chi^2(f-i)(f-j)[Q_i][Q_j] \tag{8}$$

where k_{ij} is the rate coefficient for condensation between silanol groups of sites Q_i and Q_j (of connectivities i and j, respectively). If cyclization (see below) is neglected, the rate expressions for creation and consumption of each type of site (eq 9) can be solved numerically to determine the site concentrations.

$$\frac{d[Q_i]}{dt} = \sum_j R_{(i-1)j} - \sum_j R_{ij} \tag{9}$$

Dynamic Monte Carlo Simulations Including Unlimited Cyclization. The implications of FSSE for structure development can be modeled approximately with a kinetic-Markovian model.[37] In these models, kinetic expressions are written for the evolution of a group of building blocks, and statistical expressions are used to translate the concentrations of those building blocks into predictions of average structural parameters such as molecular weight moments. For instance, Bailey et al. used silicon sites with variable numbers of hydroxyl, ethoxyl, and siloxane groups to investigate first-shell substitution effects on tetrafunctional alkoxysilane polymerization.[38] Kasehagen et al. added single small rings as building blocks.[39] Unfortunately, neither of these approaches could simulate the unusually high

conversion (82%) observed for tetraethoxysilane at gelation,[40] and so their structural predictions cannot fully match those of real silicas.

The most kinetically detailed model applied to sol−gel polymerization (and the one that we will use here) simulates the polymerization of a finite ensemble of monomers by a dynamic Monte Carlo (DMC) method.[41] In this method, one bond is added to a population of monomers per Monte Carlo step. The probability of choosing a particular type of reaction is proportional to its rate.[42] The localized rate expressions are integrated exactly as they would be for any numerical method, but the molecular weight distribution is also explicitly tracked. The method has an advantage over statistical approaches for polymer structure modeling in that the history dependence of the polymerization is correctly captured.[37,43]

DMC simulations allow not only FSSE (eq 7) but also unlimited cyclization using unimolecular-like terms.[44] Cyclization refers to the reaction between sites within the same molecule, leading to a cycle (or ring) of bonds. This reaction is often neglected in organic polymerizations,[33] but 6−10-atom cycles are well-known to be very important structural units in siloxanes.[32,40,46,49] This model is able to reproduce the gel point of tetraethoxysilane gelation, but the exact structures only approximate those of silica (only three-membered rings are allowed presently). Still, the *amount* of cyclization appears to be consistent with what might be expected in real silica sols. The concentrations of two-bond blocks, $^2B_{ij}$, with terminal sites of connectivity i and j, are determined algorithmically by counting them as they are created in the simulation. The rate of reaction of those blocks is given by eq 10, and the rate of reaction of each silicon site as the sum of the rates of bimolecular and cyclization terms (eq 11).

$$R_{ij}^{\mathrm{cyc}} = k_{3c(i,j)}\chi^2(f-i)(f-j)[^2B_{ij}] \tag{10}$$

$$\frac{\mathrm{d}[\mathrm{Q}_i]}{\mathrm{d}t} = \sum_j (R_{(i-1)j} + R_{(i-1)j}^{\mathrm{cyc}}) - \sum_j (R_{ij} + R_{ij}^{\mathrm{cyc}}) + R_{(i-1)(i-1)}^{\mathrm{cyc}} - R_{ii}^{\mathrm{cyc}} \tag{11}$$

Simulation Method. We simulated the polycondensation of 2×10^5 silicon sites on a single HP Alpha node of the NCX cluster at the University of Kentucky. Tracking the connectivities and lists of bond blocks in detail necessitated the use of the fastest processor available to us. One bond was added to a silicon site at each step of a DMC simulation (corresponding to a conversion change of $\Delta\alpha = 2.5 \times 10^{-6}$). On a local level, our simulations were equivalent to solving the set of equations (8)−(11), although the bond block concentrations were not determined analytically.

At each step of the simulation, the type of reaction was first chosen randomly with probabilities proportional to the rates of all possible reactions. The specific sites involved in the reactions were then chosen randomly from the set of sites meeting the criteria for that reaction (connectivity or potential to form cycles). For the cyclization reactions, a list of all 2-bond blocks was maintained. The number of each type of block, and each type of differently connected site, was tracked continuously to permit rate calculations.

The identities of the neighbors to each site, and the way that the sites were connected, were maintained continuously during the simulations. The polymers were not explicitly represented in 3D space, but instead as connectivity matrixes between their constituent sites. Thus, whereas the evolution of connectivities was treated exactly, diffusion was neglected (this is justified because actual gel times are on the order of months). Local steric effects on reactivity were treated in a "mean field" way through the rate coefficient dependence on site connectivity. Averaged quantities, including the number and weight-averaged degrees of polymerization, the number and weight- averaged cycle ranks, and the molecular weight distribution, were calculated periodically or continuously from the connectivities of the sites. The reduced weight-averaged degree of polymerization (DP_w^r) was calculated using the distribution of polymers with the largest single molecule left out. Below the gel point, $DP_w^r = DP_w$, but at gelation, DP_w^r suddenly drops, so a peak in DP_w^r indicates gelation.

The time elapsed during each bond addition was calculated by assuming that each reaction proceeds as an independent Poisson process (as is typically done in dynamic Monte Carlo calculations[45]):

$$\Delta t = \frac{\Delta\alpha}{\mathrm{d}\alpha/\mathrm{d}t} = \frac{2/(N_{\mathrm{Si}}f)}{2/(f[\mathrm{Si}])\sum(R_{ij} + R_{ij}^{\mathrm{cyc}})}\ln(1/x) = \frac{\ln(1/x)}{(N_{\mathrm{Si}}/[\mathrm{Si}])\sum(R_{ij} + R_{ij}^{\mathrm{cyc}})} \tag{12}$$

where N_{Si} is the number of silicon sites, α is the siloxane bond conversion, [Si] is the silicon site concentration, and x is a real number chosen randomly and uniformly from the interval (0, 1).

The bimolecular rate coefficients used were determined (see next section) by comparison to experimentally observed trends. The cyclization rate coefficients were assumed to depend on the connectivities of their ends in the same way that the bimolecular rate coefficients do (i.e., $k_{3c(i,j)} = \kappa[\mathrm{Si}]k_{ij}$ where κ is a constant). There were no limits on the number of three-site (six-atom) rings that could form during the simulations. The procedures were consistent with those of Rankin et al.[44]

Results and Discussion

Kinetic Parameters by Fitting. Before more fully elaborating the predictions of our models, we require a set of kinetic parameters consistent with the data in Figure 1. We will confine our discussion below to the results for TEOS, but the connectivity distribution of TMOS (Figure 2) is similar.

First, we show that it is possible to match the ^{29}Si NMR results fairly well with the FSSE model alone. We solved eq 9 using a fourth-order Runge−Kutta method, and manually adjusted the fitting parameters to minimize the sum of squares of the distances from the data to the model prediction. Following the experimental trend,[31] we assumed that the rate coefficients have a simplified form, as given in the caption of Table 3. Figure 3a shows the results, illustrating that it is possible to fit the connectivity distribution at least up to $\alpha = 0.6$ using the FSSE model. The parameters providing the best fit are summarized in Table 3.

When we put the kinetic parameters of the FSSE model into our DMC simulation, we observed the same connectivity distribution, but DP_w^r passed through a maximum at a conversion of only 43.8%, indicating gelation well below the experimental value. Predicting the gel conversion is at least as important as matching the connectivity distribution for an accurate model of network polymerization. Therefore, we compared the outcomes of the DMC simulations with cyclization to the connectivity distribution and adjusted the parameters to minimize the sum of the squares of the distance between the

TABLE 3: Coefficients Used for Dynamic Monte Carlo Simulations of Tetraalkoxysilane Polycondensation (Appropriate for pHCl ~ 2.5)

model	K_h[a]	k_{01}/k_{00}[b]	k_{11}/k_{00}[b]	$k_{3c(1,1)}/(k_{11}[Si])$[c]	exp (c)[b]
ideal (random branching)	18	1.0	1.0	0.0	1.0
FSSE only	18	0.7	0.14	0.0	1.0
cyclization	18	0.7	0.008	30	0.6
cages	18	0.7	0.008	1000	0.6

[a] K_h = [SiOH][ROH]/([SiOR][H_2O]). [b] For bimolecular condensation between sites of connectivity i and j, $k_{ij} = k_{00}(k_{01}/k_{00})^{[\max(i,j)-\min(i,j)]}(k_{11}/k_{00})^{\min(1,i)}e^{c(\delta_{i,3}+\delta_{j,3})}$. [c] Ratio of rate of ring closure to bimolecular growth for a linear trimer. This gives a measure of cyclization tendency.

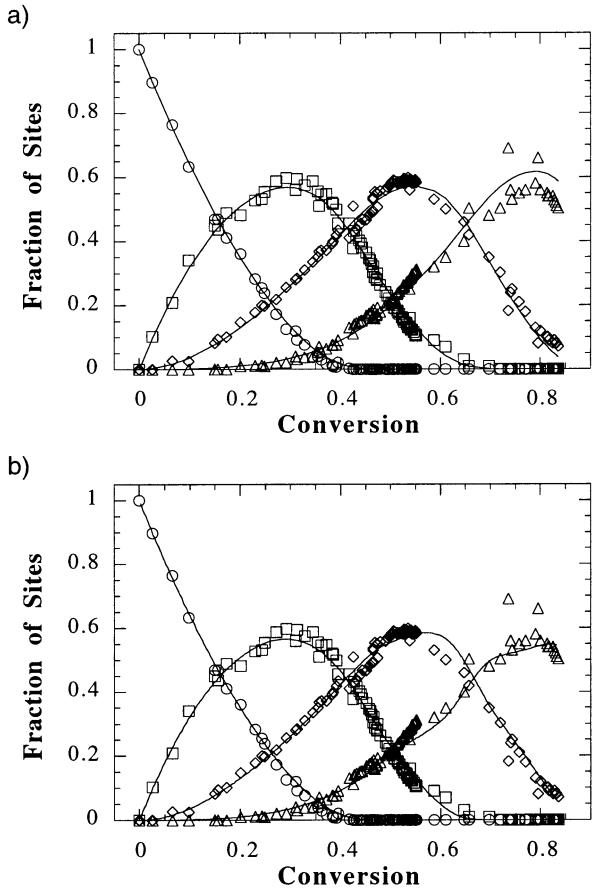

Figure 3. Results of fitting models (curves) to TEOS data (points) (a) for a model with first-shell substitution effects (FSSE) only, ignoring the gel point, and (b) for DMC simulations of 2×10^5 monomers, with matching to the experimental gel conversion of 82% also enforced. Symbols represent the same quantities as in Figure 1.

simulation results and experimental data. We also adjusted the parameters to keep the gel conversion (location of maximum DP_w^r) at 82 ± 1%.

With the same form for the bimolecular coefficients as in the FSSE case, we found that the Q_3 data could not be fit well by the DMC simulations with cyclization. Because Q_3 sites are frequently involved in cages, their mechanism of reaction may not involve inversion, and therefore the rate of reactions of Q_3 sites may differ significantly from that of other silicon sites.[46] Therefore, we multiplied the rate coefficient by a constant factor of exp(c) for each Q_3 site involved in condensation (see Table 3). This allowed the simulations to predict connectivity distributions consistent with the experiments. The resulting fit is shown in Figure 3b, and the optimal parameters are in Table 3. This is the first reported set of kinetic parameters giving results consistent with both the connectivity distribution and the gel point of TEOS starting from a monomer.

In addition to bimolecular rate coefficient and a single value of κ, we consider the dependence of α_{gel} on κ. Using DMC

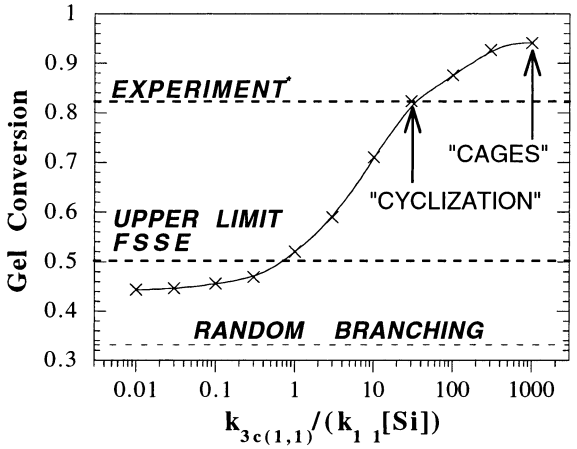

Figure 4. DMC simulated gel conversions for all bimolecular rate coefficients held constant, but the cyclization parameter varied. The "cyclization" parameter value is consistent with experiments, but the "cages" value is where the gel points have reached an upper plateau.

simulations with a different set of condensation rate coefficients, Rankin et al. found that the gel conversion shows a sigmoidal dependence on the inverse of the concentration of monomer.[44] It is known from experiments, however, that the gel conversion of TEOS changes little as the monomer concentration changes over a factor of 2.[40] The reason may be that the experimental gel conversions typically lie closer to the upper plateau in the curve, where the gel conversion changes slowly with silicon concentration.

We conducted a series of DMC simulations using the parameters found to be consistent with the connectivity distribution, but varying the monomer concentration. Figure 4 shows the result. The dimensionless cyclization rate ($\kappa = k_{3c(1,1)}/(k_{11}[Si])$) consistent with the experimental gel point is 30, but this is not where the upper plateau in the gel conversion is found. Instead, a value closer to $\kappa = 1000$ is in this plateau region. Because we are still not sure what should be the value of κ for typical silica polycondensation conditions, we will discuss the results of simulations either consistent with the silica gel point ("cyclization") or at the plateau κ value ("cages"). The upper plateau corresponds to the region where cage-like polycyclic precursors clearly form well before gelation begins.[44]

Molecular Weight Distributions. With the kinetic parameters found by fitting to experimental data, we used our DMC model to predict molecular weight distributions. Figure 5 shows how the simulated molecular weight distributions evolve with respect to conversion for each of the cases in Table 3: ideal polycondensation, polycondensation with negative FSSE, polycondensation with cyclization giving a gel conversion equal to the experimental value, and polycondensation with a very high cyclization rate.

If we compare in detail the predictions of the models, ideal polycondensation is a useful approximation very early on. Figure 5a compares the molecular weight distribution of the first three models at a siloxane bond conversion of 10%. The deviation

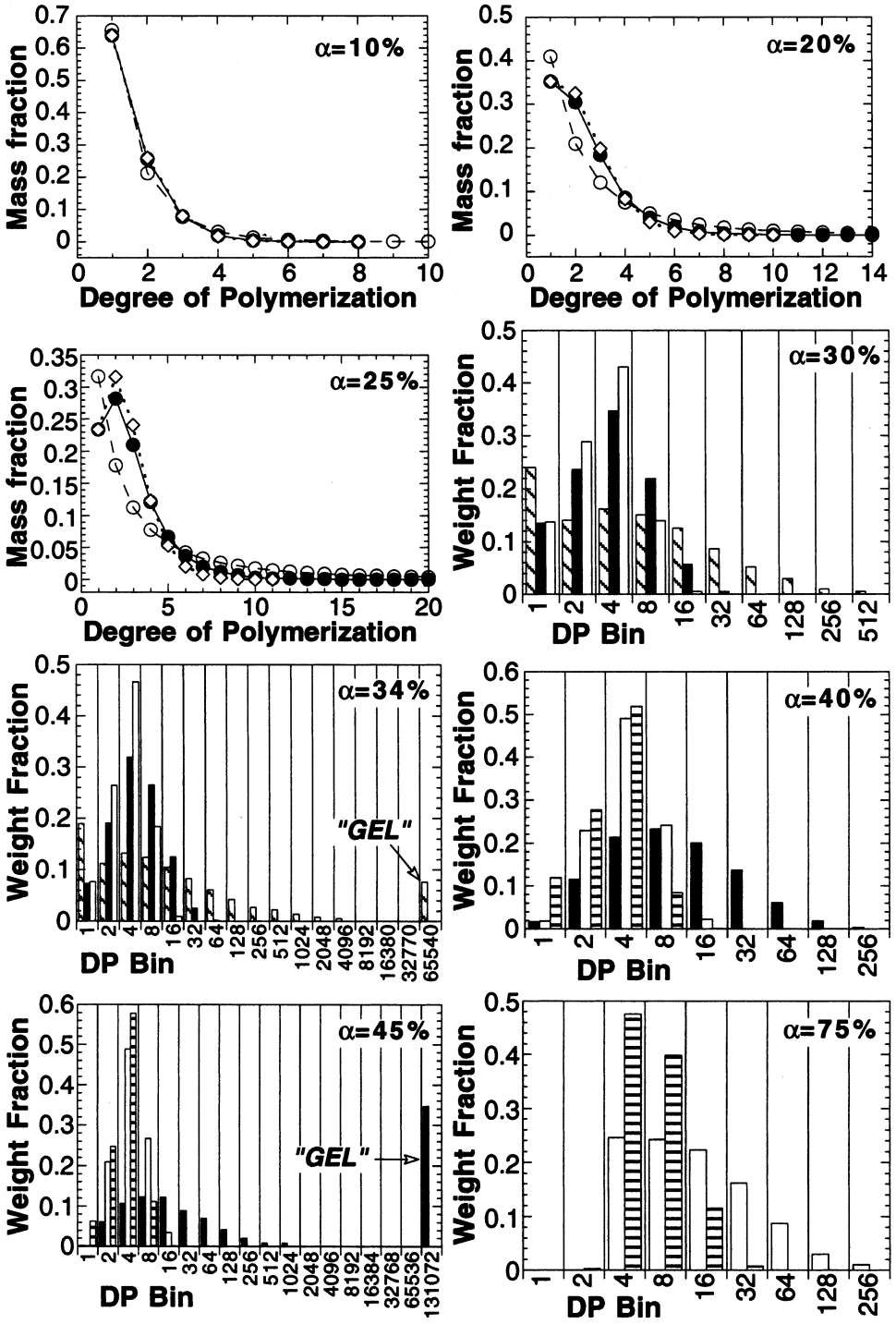

Figure 5. Comparison of simulated molecular weight distributions at (a) 10%, (b) 20%, (c) 25%, (d), 30%, (e) 34%, (f) 40%, (g) 45%, and (h) 75% siloxane bond conversion. In line plots (a)−(c), symbols represent ideal (○), FSSE (●), and cyclization (◇) models. In bar charts, fills represent ideal (diagonally lined), FSSE (black), cyclization (white), and cages (horizontally lined) models.

between them is only slight. Therefore, it is possible to predict the molecular weight distribution at $\alpha = 10\%$ (i.e., if limited water is provided, with a water-to-silicon ratio up to 0.2) using random branching. This is consistent with the connectivity distributions in Figures 1 and 2, which remain close to the ideal curves up to about this conversion.

Beyond this point, however, random branching no longer works. At 20% conversion (Figure 5b), the shape of the distribution with a negative FSSE begins to change, and by 25% conversion (Figure 5c), a peak has appeared that is not captured by the random branching model. Moving even further in conversion, Figure 5d shows that at 30% conversion, the molecular weight distribution with negative FSSE is much narrower than with random branching (note the logarithmic bin sizes in this figure). At 34% conversion, random branching already predicts gelation (a peak at very high molecular weight) whereas a narrow molecular weight distribution is still predicted by a negative FSSE (Figure 5e).

When cyclization is added, the molecular weight distribution of the model with FSSE alone are still satisfactory even at $\alpha = 25\%$, but by the time that $\alpha = 30\%$, the more low-molecular weight species accumulate when cyclization is active. The distribution with only FSSE remains broader than with cyclization at 40% conversion (Figure 5f) and by the time a conversion

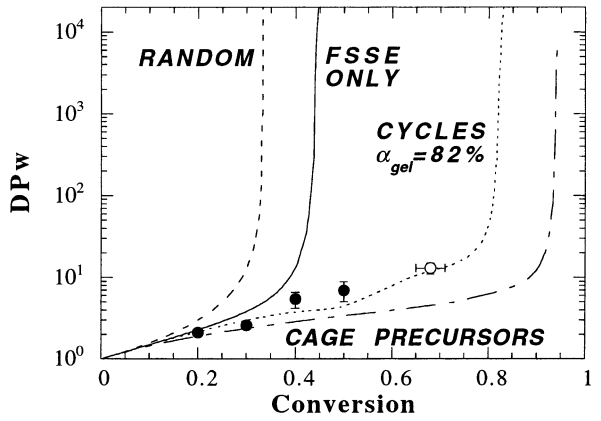

Figure 6. Simulated weight-averaged degree of polymerization as a function of siloxane bond conversion. The curves correspond, as indicated, to polycondensation with equal reactivity, with a negative first-shell substitution effect only, with cyclization and $\kappa = 30$ ($\alpha_{gel} = 82\%$), or with cyclization and $\kappa = 1000$ (which gives cage-like precursors). The points are experimental data from Grubisic-Gallot et al.[46] (○) and Kopylov et al.[45] (●). Error bars are our estimates based on the limitations of the techniques used.

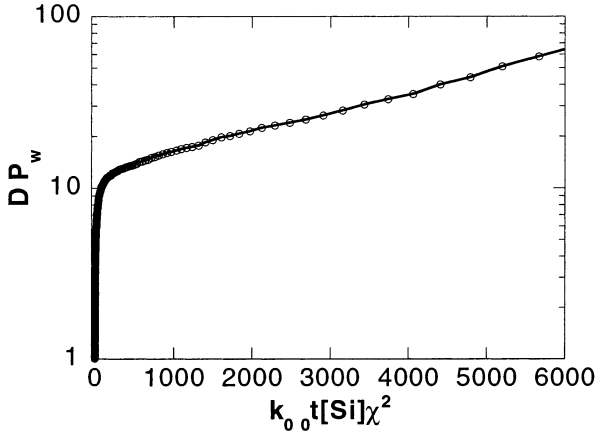

Figure 7. Weight-averaged degree of polymerization from DMC simulations with cyclization, as a function of dimensionless time.

of 45% is reached (Figure 5g), the simulations with FSSE only have gelled, whereas the distribution with cyclization is relatively narrow. At a conversion of 75% (Figure 5h), the simulations with extensive cyclization still show relatively narrow, small molecular weight distributions. With $\kappa = 30$, the gel conversion is 82%, and with $\kappa = 1000$, it reaches 93% (labeled "cages" in Figure 5). Following the trend on going from FSSE only to some cyclization, the "cages" simulation predicts an even narrower molecular weight distribution at a given conversion than the "cyclization" simulation.

The simulation results are most easily summarized by looking at the trend of weight-averaged molecular weight as a function of conversion. This trend is illustrated in Figure 6 for the four simulation models. Consistent with the observations of the full molecular weight distribution, random branching is a reasonable model up to about 10% conversion, at which point it diverges from the simulations with FSSE and cyclization. FSSE alone matches the cyclization conversion up to about 20% conversion, at which point the difference begins to grow. The two simulations with cyclization agree reasonably well up to about 50% conversion, and then the difference becomes large. Figure 6 also illustrates that the simulation results taking account of cyclization compare favorably with experimental data (points) of Kopylov et al.[47] and Grubisic-Gallot et al.[48] discussed below.

There have only been limited experimental studies of molecular weight evolution during tetraethoxysilane polymerization. Grubisic-Gallot and co-workers[48] monitored polymer size distribution using size exclusion chromatography—calibrated with polystyrene standards—and show a linear dependence of the log of the molecular weight vs time over an extended period prior to gelation. Our cyclization model exhibits qualitatively the same behavior, as illustrated in Figure 7. The molecular weight of the precursors to TEOS gels, $M_w \cong 700$ corresponding to $DP_w = 13$ at conversion $\alpha = 0.7$ and dimensionless time 200 (where the fast initial transient ends), is consistent with that extrapolated from the experimental data of Grubisic-Gallot. The time for the experimental data was scaled by $[Si][HCl]\chi^2$, as would be expected for acid-catalyzed polycondensation, and the molecular weight was extrapolated to zero time. Although the extrapolated results are consistent, we cannot directly compare the time scale of DMC simulations to the experimental one, because at high conversions ($\alpha > 0.7$) the kinetics is driven primarily by condensation of Q_3 sites, and the corresponding rate coefficients k_{33} and k_{23} show a different pH dependence than other sites (see below).

We also compare how the predicted degree of polymerization and concentration of the first few oligomers match those reported by Kopylov et al. Figure 8 shows that our simulations accurately capture the ranges of conversions where respective species are present. Deviations in concentration magnitudes may be due to differences in the sample preparation procedures of Kopylov et al., because the monomer and water concentrations are lower than those used for ^{29}Si NMR (the filled circles in Figure 8). However, mass weighted degrees of polymerization calculated from data reported by Kopylov are in a good agreement with simulation results (Figure 6), which is an encouraging validation of our predictions.

In many instances, the siloxane bond conversion is still not readily available, so another useful correlation is the dependence of DP_w on the monomer consumption for conversions where the monomer is present. We show the simulation results in Figure 9. The ratio of the monomer concentration to the initial monomer concentration can be determined during alkoxysilane polymerization by molybdic acid titration,[49] gas chromatography, or NMR. Results of cyclization and cage models differ only little in this range of conversions ($\alpha < 0.35$), so that Figure 9 can be used to estimate the silica DP_w values up to 4. When the monomer conversions from ^{29}Si NMR are used as the *x*-axis, the agreement is good between our simulations and DP_w from Kopylov et al.[47] (Figure 9).

pH Effects. Finally, we briefly comment on how the pH affects condensation rate coefficients. The monomer−monomer condensation rate coefficient (k_{00}) is well-known to increase monotonically with [HCl] for $[HCl] \geq 0.0001$.[50] Condensations of silanol groups at Q_0, Q_1, and Q_2 sites are acid-catalyzed electrophilic substitutions at pH values below their respective isoelectric points (IEP). Because we estimate all of their IEPs to be above ~3, the condensation rate coefficients k_{ij} involving Q_0, Q_1, and Q_2 sites are expected to increase linearly with [HCl] for pHCl < 3. Q_3 sites are a different case, because their IEP and thus the minimum in condensation rate are around 2. Several investigations of the dependence of silica gel time on pH have been reported (e.g., Grubisic-Gallot et al.). Whereas the absolute values reported in various investigations differ due to changes in monomer type, silicon concentration, or temperature, a maximum gel time is observed near pH 2 in all cases, with the gel time decreasing (i.e., the apparent gelation rate increasing) with pH between 2 and 4. The most reasonable interpretation of the gel times is, therefore, that they most accurately reflect the condensation kinetics of Q_3 sites. However, condensation

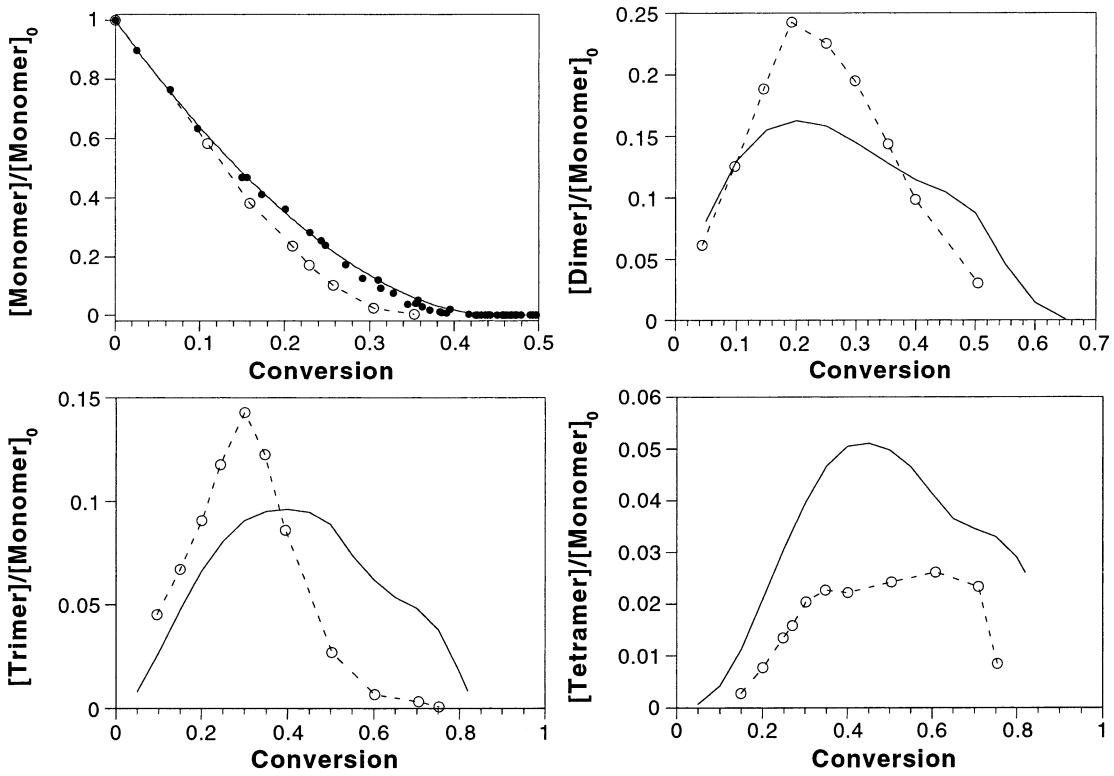

Figure 8. Comparison of "cyclization" DMC results (solid curves) to data (open circles with dashed lines) of Kopylov et al.[47] for tetraethoxysilane polycondensation. The filled circles in the monomer figure are the collected data from ^{29}Si NMR (Figure 1).

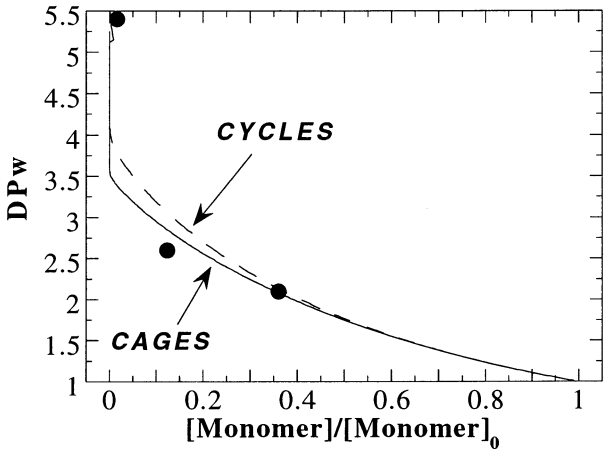

Figure 9. Simulated weight-averaged degree of polymerization as a function of monomer consumption for the same cases as in Figure 6. This plot can be compared to molybdic acid titration results. The *x* axis of the experimental data is corrected to be the monomer fraction at a given conversion from ^{29}Si NMR. Points are data of Kopylov et al.[47]

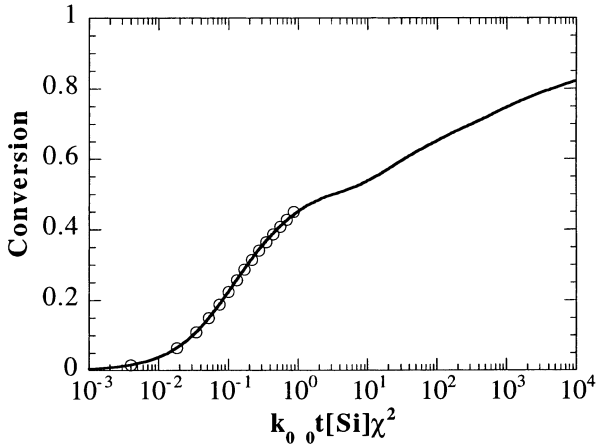

Figure 10. Calculated conversion vs dimensionless time for FSSE and DMC simulations. Both calculations agree up to conversion 0.45, at which point the FSSE model predicts that gelation occurs.

of Q_3 sites is only important at conversions greater than 0.5, so for conversions below 0.5 (where few Q_3 sites are present) we can predict real-time kinetics well (cf. Sanchez et al.[29]) using condensation rate coefficients from Table 3 (FSSE and cyclization models) with time scaled by $k_{00}[\mathrm{Si}]\chi^2$ (Figure 10).

As the conditions are changed from those outlined above ($1 < \mathrm{pHCl} < 3$) giving homogeneous gels, the structure of the gels generated from pure silica changes. Previously observed connectivity distributions at pHCl 3.1 and 3.3[35] are consistent with a less-negative FSSE as the pHCl increases, with near-ideal distribution at $\mathrm{pHCl} = 3.3$. Gels become less homogeneous to the naked eye and can be shown to be composed of larger particles. It is well-known that at neutral and mildly basic pH (e.g., ammonia catalyzed Stöber process), nucleation, growth and aggregation models are appropriate to describe the formation of silica particles.

On the other hand, at high acid concentrations ($\mathrm{pHCl} < 1$) one has to consider condensation reversibility (siloxane bond hydrolysis) possibly modifying the kinetics and structure of silica oligomers produced by irreversible condensation process considered here. Moreover, at water starved conditions, a substantial fraction of water can be tied up in hydration of the strong acid. At water/silicon < 1 and $\mathrm{pHCl} = 1$ one gets water/HCl < 20, so that assuming common hydration numbers, ca. 50% of water molecules can be in the first hydration shell of H_3O^+ and Cl^- ions. Because of complications at low and high pH, we cannot yet extend our predictions outside of the homogeneous gel region. Because the choice of synthesis pH can be motivated by factors besides silica polymerization (e.g., chemical stability of biological additives), quantitative modeling of "cloudy" silica gel formation remains an important challenge.

Conclusions

Summarizing previously published ^{29}Si NMR data on hydrolytic polycondensation of alkoxysilanes, we find that the evolution of the connectivity distribution with respect to conversion is consistent across a range of moderately acidic synthesis conditions. Although first-shell substitution effects (FSSE) alone are enough to match the connectivity distribution, we are able to match both the connectivity distribution and the experimentally observed gel conversion for tetraethoxysilane only with dynamic Monte Carlo (DMC) simulations with extensive cyclization.

Using kinetic parameters determined by fitting our models to experimental data, we predict the size of silica building blocks present at each stage of the polymerization process and specify when simplified models are applicable. Random branching theory can be used to analyze the polymerization below a conversion of 10%. A model with FSSE alone is sufficient for conversions less than 25%. Beyond that, extensive cyclization is needed to predict the formation of a distribution of polycyclic species from which a gel actually forms. The molecular weight distribution remains narrow and insensitive to the assumed cyclization rate up to a conversion of 50%, indicating the formation of a distribution of cage-like precursors. The predicted building block distributions show encouraging similarities with experimental measurements and can be refined by allowing more types of rings to form.

The calculated molecular weight distributions provide a road map for the size control of silica building blocks at each stage of the polycondensation process, where a measure of the siloxane bond conversion (for instance, from FTIR) can be used as a monitoring variable. We suggest that this road map can be used to design polymerization processes for nanocomposites of silica combined with other components to obtain materials such as mixed metal catalysts and organic−inorganic hybrids.

Acknowledgment. S.R. acknowledges a grant of computer time from the University of Kentucky Center for Computational Sciences for the DMC simulations in this work and partial support from the University of Kentucky Research Challenge Trust Fund.

References and Notes

(1) Kresge, C. T.; Leonowicz, M. E.; Roth, W. J.; Vartuli, J. C.; Beck, J. S.; *Nature* **1992**, *359*, 710.

(2) Brinker, C. J.; Scherer, G. W. *Sol−gel Science*: *The Physics and Chemistry of Sol−Gel Processing*; Academic: Boston, 1990.

(3) Higgins, J. B. In *Reviews in Mineralogy*, *Volume 29*: *Silica. Physical Behavior, Geochemistry and Materials Applications*; Heaney, P. J., Prewitt, C. T., Gibbs, G. V., Eds.; Mineralogical Society of America: Washington, DC, 1994; pp 507−544.

(4) Ying, J. Y.; Mehnert, C. P.; Wong, M. S. *Angew. Chem., Int. Ed. Engl.* **1999**, *38*, 56.

(5) Dabbs, D. M.; Aksay, I. A. *Annu. Rev. Phys. Chem*. **2000**, *51*, 601.

(6) Sanchez, C.; Ribot, F. *New J. Chem.* **1994**, *18*, 1007. Judeinstein, P.; Sanchez, C. *J. Mater. Chem.* **1996**, *6*, 511. Laine, R. M., Sanchez, C., Giannelis, E., Brinker, C. J., Eds. *Organic/Inorganic Hybrid Materials − 2000*; Materials Research Society: Pittsburgh, PA, 2000.

(7) Nakanishi, K.; Soga, N. *J. Non-Cryst. Solids* **1992**, *139*, 1−13 and 14−24; *142*, 36−44 and 45−54.

(8) Tanabe, K.; Sumiyoshi, T.; Shibata, K.; Kiyoura, T.; Kitagawa, J. *Bull. Chem. Soc. Jpn.* **1974**, *47*, 1064. Kung, H. H. *J. Solid State Chem.* **1984**, *52*, 191.

(9) Schneider, M.; Baiker, A. *Catal. Rev.−Sci. Eng.* **1995**, *37*, 515. Ward, D. A.; Ko, E. I. *Ind. Eng. Chem. Res.* **1995**, *34*, 421.

(10) Livage, J.; Henry, M.; Sanchez, C. *Prog. Solid State Chem.* **1988**, *18*, 259.

(11) Miller, J. B.; Rankin, S. E.; Ko, E. I. *J. Catal.* **1994**, *148*, 673. Miller, J. B.; Johnston, S. T.; Ko, E. I. *J. Catal.* **1994**, *150*, 311. Miller, J. B.; Ko, E. I. *J. Catal.* **1995**, *153*, 194. Pozarnsky, G. A.; McCormick, A. V. *J. Non-Cryst. Solids* **1995**, *190*, 212.

(12) Sanchez, J.; McCormick, A. V. *J. Phys. Chem*. **1992**, *96*, 8973.

(13) Rankin, S. E.; Šefčik, J.; McCormick, A. V. *Ind. Eng. Chem. Res.* **1999**, *38*, 3191.

(14) Rankin, S. E.; McCormick, A. V. *Chem. Eng. Sci.* **2000**, *55*, 1955.

(15) Devreux, F.; Boilot, J. P.; Chaput, F. *Phys. Rev. A* **1990**, *41*, 6901.

(16) Brinker, C. J.; Raman, N. K.; Logan, M. N.; Seghal, R.; Assink, R. A.; Hua, D. W.; Ward, T. L. *J. Sol-Gel Sci. Technol.* **1995**, *4*, 117.

(17) Brinker, C. J.; Assink, R. A. *J. Non-Cryst. Solids* **1989**, *111*, 48.

(18) Kelts, L. M.; Effinger, N. J.; Melpolder, S. M. *J. Non-Cryst. Solids* **1986**, *83*, 353.

(19) Brunet, F.; Cabane, B.; Dubois, M.; Perly, B. *J. Phys. Chem*. **1991**, *95*, 945.

(20) VanBeek, J. J.; Seykens, D.; Jansen, J. B. H. *J. Non-Cryst. Solids* **1992**, *146*, 111.

(21) Brunet, F.; Cabane, B. *J. Non-Cryst. Solids* **1993**, *163*, 211.

(22) Assink, R. A.; Kay, B. D. *J. Non-Cryst. Solids* **1988**, *107*, 35.

(23) Nishida, F.; McKiernan, J. M.; Dunn, B.; Zink, J. I.; Brinker, C. J.; Hurd, A. J. *J. Am. Chem. Soc.* **1995**, *78*, 1640.

(24) Flory, P. J. *J. Am. Chem. Soc.* **1941**, *63*, 3083, 3091, and 3096.

(25) Stockmayer, W. H. *J. Chem. Phys*. **1943**, *11*, 45; *12*, 125.

(26) Klemperer, W. G.; Ramamurthi, S. D. *J. Non-Cryst. Solids*, **1990**, *121*, 16.

(27) Bechtold, M. F.; Vest, R. D.; Plambeck, L. *J. Am. Chem. Soc*. **1968**, *90*, 4590.

(28) Pope, E. J. A.; Mackenzie, J. D. *J. Non-Cryst. Solids* **1988**, *101*, 198.

(29) Sanchez, J.; Rankin, S. E.; McCormick, A. V. *Ind. Eng. Chem. Res.* **1996**, *34*, 117.

(30) Vainrub, A.; Devreux, F.; Boilot, J. P.; Chaput, F.; Sarkar, M. *Mater. Sci. Eng. B* **1996**, *37*, 197.

(31) Rankin, S. E.; Macosko, C. W.; McCormick, A. V. *AIChE J*. **1998**, *44*, 1141.

(32) Rankin, S. E.; Macosko, C. W.; McCormick, A. V. *Chem. Mater*. **1998**, *10*, 2037.

(33) Flory, P. J. *Principles of Polymer Chemistry*; Cornell University Press: Ithaca, NY, 1953.

(34) Dotson, N. A.; Galván, R.; Laurence, R. L.; Tirrell, M. T. *Polymerization Process Modeling*; Wiley VCH: New York, 1996.

(35) Pouxviel, J. C.; Boilot, J. P.; Beloeil, J. C.; Lallemand, J. Y. *J. Non-Cryst. Solids* **1987**, *89*, 345.

(36) Kay, B. D.; Assink, R. A. *J. Non-Cryst. Solids* **1988**, *104*, 112.

(37) Sarmoria, C.; Miller, D. R. *Macromolecules* **1991**, *24*, 1833.

(38) Bailey, J. K.; Macosko, C. W.; Mecartney, M. L. *J. Non-Cryst. Solids* **1990**, *125*, 208.

(39) Kasehagen, L. J.; Rankin, S. E.; McCormick, A. V.; Macosko, C. W.; *Macromolecules* **1997**, *30*, 3921.

(40) Ng, L. V.; Thompson, P.; Sanchez, J.; Macosko, C. W.; McCormick, A. V. *Macromolecules* **1995**, *28*, 6471.

(41) Šomvársky, J.; Dušek, K. *Polym. Bull* **1994**, *33*, 369.

(42) Gillespie, D. T. *J. Comput. Phys*. **1976**, *22*, 403.

(43) Hendrickson, R. C.; Macosko, C. W.; Gupta, A. M. *J. Comput. Polym. Sci.* **1994**, *4*, 53.

(44) Rankin, S. E.; Kasehagen, L. J.; McCormick, A. V.; Macosko, C. W.; *Macromolecules* **2000**, *33*, 7639.

(45) Fichthorn, K. A.; Weinberg, W. H. *J. Chem. Phys*. **1991**, *95*, 1090.

(46) Klemperer, W. G.; Mainz, V. V.; Millar, D. M. *Mater. Res. Soc. Symp. Proc*. **1986**, *73*, 3.

(47) Kopylov, V. M.; Voronkov, A. V.; Zinovich, S. K.; Tseitlin, G. M.; Kireyev, V. V.; Kostylev, I. M. *Polym. Sci. USSR* **1985**, *27*, 385.

(48) Grubisic-Gallot, Z.; Schosseler, F.; Lixon, P.; Cabane, B. *Macromolecules* **1992**, *25*, 3733.

(49) Iler, R. K. *The Chemistry of Silica*: *Solubility, Polymerization, Colloid and Surface Properties and Biochemistry*; Wiley: New York, 1979.

(50) Šefčik, J.; McCormick, A. V. *Catal. Today* **1997**, *35*, 205.